Ultrasound in Med. & Biol., Vol. 39, No. 12, pp. 2333–2341, 2013

0301-5629/$ - see front matter

http://dx.doi.org/10.1016/j.ultrasmedbio.2013.07.006

● *Original Contribution*

CHARACTERIZATION OF THYROID CANCER IN MOUSE MODELS USING HIGH-FREQUENCY QUANTITATIVE ULTRASOUND TECHNIQUES

ROBERTO J. LAVARELLO,* WILLIAM R. RIDGWAY,† SANDHYA S. SARWATE,† and MICHAEL L. OELZE†

*Laboratorio de Imagenes Medicas, Seccion Electricidad y Electronica, Pontificia Universidad Catolica del Peru, Lima, Peru; and †Bioacoustics Research Laboratory, Department of Electrical and Computer Engineering, University of Illinois at Urbana-Champaign, Urbana, Illinois, USA

(*Received* 27 *November* 2012; *revised* 28 *June* 2013; *in final form* 15 *July* 2013)

Abstract—Currently, the evaluation of thyroid cancer relies on the use of fine-needle aspiration biopsy, as non-invasive imaging methods do not provide sufficient levels of accuracy for the diagnosis of this disease. In this study, the potential of quantitative ultrasound methods for characterization of thyroid tissues was studied using a rodent model *ex vivo*. A high-frequency ultrasonic scanning system (40 MHz) was used to scan thyroids extracted from mice that had spontaneously developed thyroid lesions (cancerous or benign). Three sets of mice were acquired having different predispositions to developing three thyroid anomalies: C-cell adenoma, papillary thyroid carcinoma (PTC) and follicular variant papillary thyroid carcinoma (FV-PTC). A fourth set of mice that did not develop thyroid anomalies (normal mice) were used as controls. The backscatter coefficient was estimated from excised thyroid lobes the different mice. From the backscatter coefficient versus frequency (25–45 MHz), the effective scatterer diameter (ESD) and effective acoustic concentration (EAC) were estimated. From the envelope of the backscattered signal, the homodyned K distribution was used to estimate the k parameter (ratio of coherent to incoherent signal energy) and the μ parameter (number of scatterers per resolution cell). Statistically significant differences were observed between cancerous thyroids and normal thyroids based on the ESD, EAC and μ parameters. The mean ESD values were 18.0 ± 0.92, 15.9 ± 0.81 and 21.5 ± 1.80 μm for the PTC, FV-PTC and normal thyroids, respectively. The mean EAC values were 59.4 ± 1.74, 62.7 ± 1.61 and 52.9 ± 3.42 dB (mm^{-3}) for the PTC, FV-PTC and normal thyroids, respectively. The mean μ values were 2.55 ± 0.37, 2.59 ± 0.43 and 1.56 ± 0.99 for the PTC, FV-PTC and normal thyroids, respectively. Statistically significant differences were observed between cancerous thyroids and C-cell adenomas based on the ESD and EAC parameters, with an estimated ESD value of 21.3 ± 1.50 μm and EAC value of 54.7 ± 2.24 dB mm^{-3} for C-cell adenomas. These results suggest that high-frequency quantitative ultrasound may enhance the ability to detect and classify diseased thyroid tissues. (E-mail: oelze@illinois.edu)

Key Words: **Quantitative ultrasound, Tissue characterization, Cancer diagnosis, Thyroid.**

INTRODUCTION

Thyroid nodules are a very common occurrence and present challenges to clinical diagnosis. In the United States, between 4% and 7% of the general population have clinically palpable nodules (Lewis et al. 2002). The American Cancer Society (2012) estimated in 2012 there would be 56,460 new cases of thyroid cancer. Although the prognosis in thyroid cancer is relatively good, with 20-y survival rates of around 90% (Cotran et al. 1999), clearly differentiating between benign and malignant nodules is problematic. Using ultrasonic imaging, certain studies have predicted that up to 70% of the adult population have detectable thyroid nodules (Marqusee et al. 2000; Ross 2002; Tan and Gharib 1997). With the increased use of ultrasound to image the head and neck, the management problem has skyrocketed over the past few decades to epidemic proportions. The number of incidentally found nodules on ultrasound examinations of asymptomatic patients has complicated the debate on proper management of thyroid nodules (Chidiac and Aron 1997; Leinung et al. 2001; Mirilas and Skandalakis 2002).

The problem of thyroid cancer management is usually one of diagnosis rather than detection. Clinicians will take a conservative approach if there is a modest level of suspicion of malignancy in detected thyroid nodules.

Address correspondence to: Michael L. Oelze, Bioacoustics Research Laboratory, Department of Electrical and Computer Engineering, University of Illinois at Urbana-Champaign, 405 North Mathews, Urbana, IL 61801, USA. E-mail: oelze@illinois.edu

This results in many fine-needle aspiration biopsies with a benign diagnosis and many with an undetermined diagnosis or just a level of suspicion. As a result, there are many unnecessary surgical procedures in hindsight and testing and treatments that carry with them their own set of risks (Silver and Parangi 2004).

Although the advent of ultrasonography of the thyroid has contributed to the management crisis concerning the prevalence of nodules in asymptomatic adults, it has been used to alleviate some of the costs and burden associated with proper management. Abundant research has been conducted to determine the ability of ultrasonic imaging to predict the malignancy of thyroid nodules with some success (Ahuja and Metreweli 2000; Ahuja and Ying 2002; Brander et al. 2000; Chan et al. 2003; Frates et al. 2003; Kim et al. 2002; Koike et al. 2002; Liebeskind et al. 2005; Papini et al. 2002). The diagnostic approach of ultrasound currently falls under two branches: ultrasonographic features (*i.e.*, echogenicity of the nodule, type of border around the nodule, presence or absence of calcifications, composition and size) and color Doppler characteristics of the nodules (Ahuja and Metreweli 2000).

Several studies using these ultrasonic features have yielded a variety of results. The majority of the results in the literature, however, suggest that current ultrasonic imaging methods may provide only a level of suspicion for a particular nodule (Frates et al. 2003; Iannuccilli et al. 2004; Moon et al. 2008; Papini et al. 2002). This is reflected in the current guidelines provided by the American Thyroid Association, which state that no single sonographic feature or combination of features has sufficient sensitivity and specificity to allow for non-invasive diagnosis of all thyroid nodules and, therefore, recommend fine-needle aspiration as the procedure of choice in the evaluation of thyroid nodules (Cooper et al. 2009).

Another difficulty with the use of sonographic and color Doppler features to diagnose thyroid nodules is the lack of system independence. The ability to map out the feature set is highly dependent not only on the equipment used, but also on the operator and the training of the operator. As a result, the statistics of sonographic feature detection vary from one study to the next. In the end, accurate diagnosis comes from a cellular level (optical microscopy), and the feature sets proposed using conventional ultrasound diagnosis have little basis in structure at the cellular level.

Recently, elastography techniques involving ultrasound have been examined for their ability to improve thyroid cancer diagnostics. In one study, shear wave elastography was used to diagnose 146 nodules from 93 patients (Sebag et al. 2010). The use of shear wave elastography and the ultrasound features of the thyroids had a sensitivity of 81.5% and specificity of 97.0%. Similar experiments using strain imaging were observed to increase the sensitivity and specificity over ultrasound B-mode imaging alone (Rago et al. 2010). Ultrasound elastography has been used to correlate the stiffness of thyroid nodules to malignancy, where increased stiffness of thyroid nodules is associated with cancer and decreased stiffness is associated with benign nodules (Vorlander et al. 2010). These techniques show promise, but still need to be evaluated in larger clinical studies.

Another ultrasonic imaging mode that can potentially improve thyroid cancer diagnosis and help alleviate the management crisis resulting from the detection of thyroid nodules is quantitative ultrasound (QUS) techniques based on ultrasound backscatter. QUS techniques (spectral-based parameters and parameters based on envelope statistics) have been used to characterize different disease states such as prostate cancer, ocular tumors, mammary cancer in rodent models, micrometastases in lymph nodes and fatty liver disease (Feleppa et al. 1997; Ghoshal et al. 2012; Lizzi et al. 1997; Mamou et al. 2011; Oelze et al. 2004; Silverman et al. 2003).

On the basis of these earlier successes, where changes in tissue microstructure led to new sources of image contrast using QUS parameters, it is possible that high-frequency QUS could also provide sources of image contrast to detect and classify thyroid cancer. Studies of QUS applied to thyroid imaging are, however, sparse. Scatterer size imaging was used to examine a couple of cases of thyroid cancer in Wilson et al. (2006), and preliminary data suggested that scatterer size imaging could increase contrast between thyroid abnormalities and healthy thyroid tissue. However, no subsequent correlation with pathology provided a comparison between actual underlying microstructure and the values of the lone QUS parameter analyzed in that study. The few studies on quantitative envelope characterization are based on texture analysis (Catherine et al. 2006; Rajendra et al. 2012) instead of envelope statistics parameters, which are more closely connected to tissue microstructure (Destrempes and Cloutier 2010).

In this study on mouse models of thyroid cancer, multiple QUS parameters based on the frequency-dependent backscatter coefficient and the envelope statistics of the backscattered ultrasound were estimated. These QUS estimates were then compared with histologic slides of the thyroid tissues analyzed.

METHODS

The experimental protocol was approved by the Institutional Animal Care and Use Committee of the University of Illinois at Urbana-Champaign and satisfied

all university and National Institutes of Health rules for the humane use of laboratory animals.

A high-frequency ultrasonic scanning system was used to scan thyroids extracted from mice that had spontaneously developed thyroid lesions (cancerous or benign): one set of control mice and three sets of mice with different predispositions to developing thyroid anomalies. The first set of mice (n = 8) did not develop thyroid lesions, were judged to have normal thyroids by a pathologist and were used as controls. The second set of mice (n = 6) of the Rb 1+/– mouse strain was acquired from the mouse cancer model repository at the National Cancer Institute (courtesy of the Jacks Lab at the Koch Institute for Integrative Cancer Research at Massachusetts Institute of Technology) (Jacks et al. 1992). Approximately 50% of these mice develop C-cell adenomas or C-cell hyperplasia of the thyroid. These growths are typically benign in nature. The third set of mice (n = 6) from the TG-BRAF mouse line was acquired from the Fagin lab (Sloan-Kettering Institute for Cancer Research) (Knauf et al. 2005). These mice develop papillary thyroid carcinomas (PTCs). The fourth set of mice (n = 5) was acquired from Dr. Cheng's lab (Center for Cancer Research, NIH) (Suzuki et al. 2002) and consisted of mutant mice in which a dominant negative mutant thyroid nuclear receptor gene, TRβPV, had been introduced into the TRβ gene locus. As a result of this mutation, as the TR$\beta^{PV/PV}$ mice aged, they developed metastatic thyroid tumors consistent with follicular variant papillary thyroid carcinoma (FV-PTC).

All mice were examined weekly and scanned with a VisualSonics Vevo 2100 (VisualSonics, Toronto, ON, Canada) to determine the size of the thyroid of a particular mouse, or if a mouse had developed a detectable lesion in the thyroid. When the thyroid was determined to be larger than normal, or appeared to have lesions, the mouse was taken for experimental examination using the QUS scanning system and analysis.

Mice selected for scanning were euthanized, and both thyroid lobes were extracted along with a portion of the trachea. The thyroid lobes were placed in a tank of de-gassed 0.9% saline maintained at 37°C for ultrasonic scanning. After scanning, both thyroid lobes were excised, fixed in 10% neutral buffered formalin, processed and embedded in paraffin, sectioned and stained for routine histologic evaluation by light microscopy. A diagnosis was obtained for all animals after histopathologic evaluation.

The QUS scanning system consisted of a weakly-focused (f/3) single-element transducer (USC, Ultrasonic Transducer Resource Center, Los Angeles, CA, USA) with nominal center frequency of 40 MHz (the actual –6-dB bandwidth of the transducer was 25–45 MHz) and active element diameter of 3 mm. The transducer was operated using a Panametrics 5900 pulser/receiver (Olympus NDT, Waltham, MA, USA). Backscattered waveforms were acquired with a PC *via* a 14-bit UF3-4121 A/D card with 250-MHz sampling (Strategic Test, Woburn, MA, USA) and were saved to a computer for post-processing. For most thyroids, more than a dozen slices were acquired by translating the transducer using a micro-positioning system (Daedal, Harrisburg, PA, USA) controlled with custom LabView (National Instruments, Austin, TX, USA) software. Slices were taken 0.2 to 0.4 mm apart (larger than a beamwidth) across the thyroid and perpendicular to the axial direction of the trachea. For each slice, a number of scan lines were acquired depending on the size of the thyroid. Scan lines were separated by 0.05 mm, that is, approximately half a beamwidth at the transducer center frequency.

From the scan lines, the envelope was detected and a B-mode image was constructed of the thyroid lobes. For processing, custom MATLAB (MathWorks, Natick, MA, USA) software was used to draw regions of interest in each slice corresponding to the actual thyroid lobes. Within the regions of interest, data blocks were automatically selected for QUS analysis. Each data block was 0.5×0.5 mm with a 75% overlap in the axial and lateral directions. Two QUS parameters were examined based on the backscatter coefficient versus frequency (spectral-based parameters: effective scatterer diameter [ESD] and effective acoustic concentration [EAC]) and two QUS parameters were estimated from the envelope statistics (k and μ).

From each data block, the backscatter coefficient versus frequency was estimated by the method of Chen et al. (1997) and based on studies by Lavarello et al. (2011). For calculation of the backscatter coefficient, a reference spectrum for each depth location was acquired by measuring the signal reflected from a smooth planar surface of known reflectivity (Plexiglas). To correct for attenuation, values of attenuation for different thyroids were estimated using insertion loss techniques. The mean attenuation slope value from the estimates for all the thyroids in the frequency range 25–45 MHz was 1.19 ± 0.256 dB/MHz/cm, and this value was used for attenuation compensation when calculating the backscatter coefficient. Similar values of attenuation in human thyroids have been estimated, that is, 0.91–1.5 dB/MHz/cm when operating at 10 MHz (Fuji et al. 2003).

Spectral-based parameters were estimated by applying a spherical Gaussian model to the data and using an estimator that has been described previously (Insana et al. 1990; Oelze et al. 2002). Under plane wave incidence and no multiple scattering assumptions, the backscatter coefficient (BSC) can be modeled as

$$BSC(f) = 2.89LqEAC\frac{f^4ESD^6}{1+0.67(fqESD)^2}e^{-3.04f^2ESD^2}$$

where f is the frequency in megahertz, L is the gate length in millimeters, and q is the ratio of the aperture radius to data block depth. From a physical point of view, ESD is indicative of the size of the scatterers giving rise to the measured ultrasonic echoes, and EAC is proportional to both the number density of scatterers and the square of the impedance mismatch between the scatterers and background. In this work, the analysis bandwidth used for deriving the spectral-based parameters was 25–45 MHz.

Envelope statistics were estimated with a routine used to parameterize the homodyned K distribution (Hruska and Oelze 2009). The envelope of the backscattered signal was detected, and the values of the envelope corresponding to a particular data block were stored in a vector. The signal-to-noise ratio, skewness and kurtosis were calculated from the envelope amplitude values in the data block vector corresponding to two fractional-order moments (*i.e.,* 0.72 and 0.88). Level curves previously stored for values of signal-to-noise ratio, skewness and kurtosis were generated for k and μ parameters for each fractional-order moment. The intersection of the curves in the k–μ space represented the values obtained for the particular data block. In our estimator, μ parameter estimates greater than 10 were excluded because these values were found to be

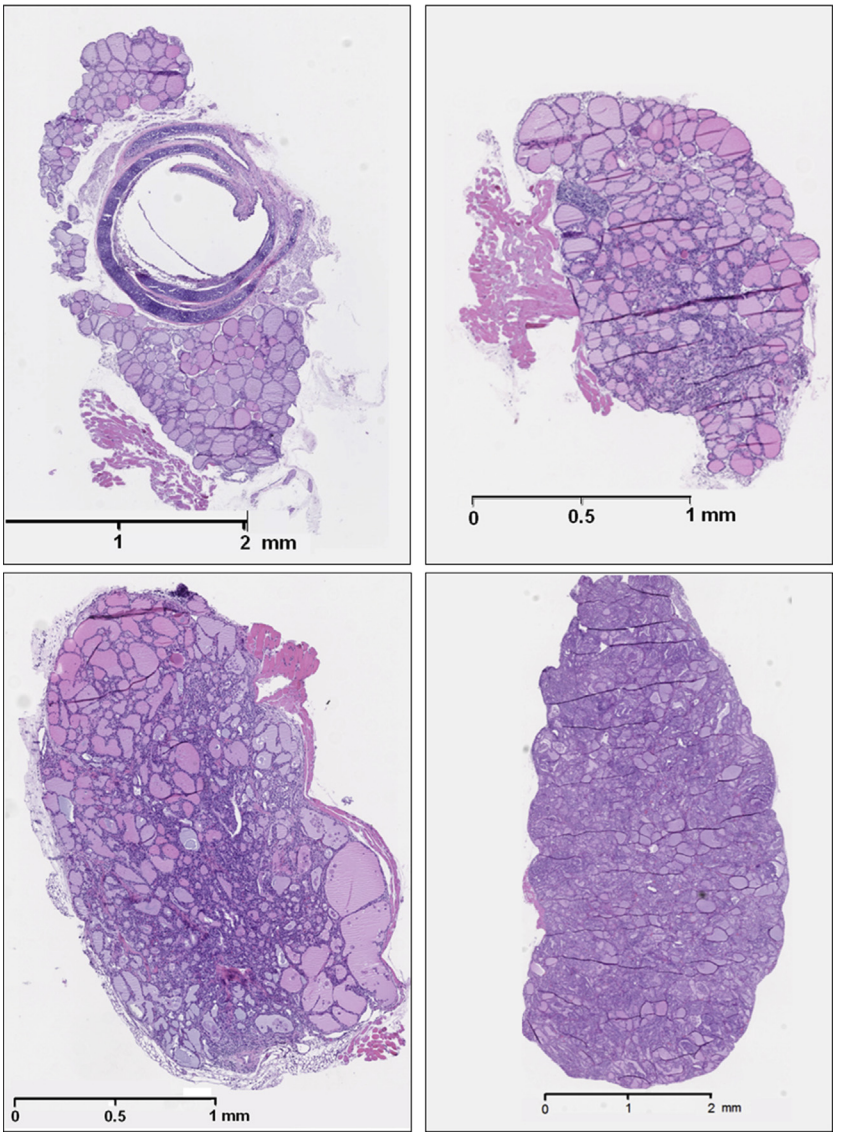

Fig. 1. Histology images of (top left) normal thyroid, (top right) C-cell adenoma, (bottom left) papillary thyroid carcinoma and (bottom right) follicular variant papillary thyroid carcinoma.

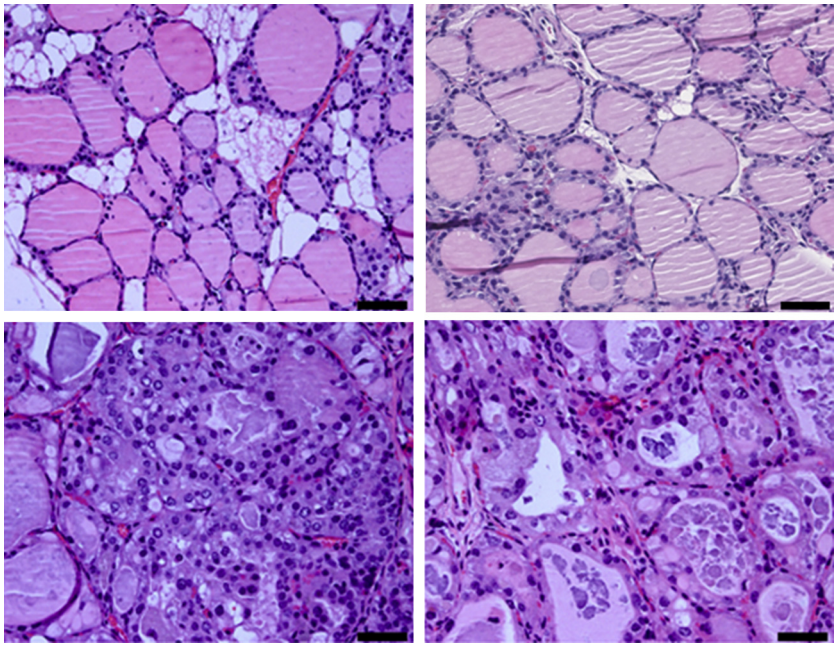

Fig. 2. High-power views (40×) of (top left) normal thyroid, where the round to oval follicles contain colloid material and benign fatty tissue separates groups of follicles; (top right) C-cell neoplasm; (bottom left) papillary thyroid carcinoma; and (bottom right) follicular variant papillary thyroid carcinoma. Scale bar = 50 μm.

unreliable estimates (Hruska 2009). The k parameter quantifies the ratio of the coherent scattering signal to the incoherent scattered signal. If scatterers are regularly spaced or large single scatterers are present, k will increase. The μ parameter provides an estimate of the number of scatterers per resolution cell. If the resolution cell of the imaging system can be estimated, then an estimate of the number density of scatterers can be obtained. Because these parameters are related to the organization of underlying scatterers, it may be possible to correlate these parameters to underlying structure.

RESULTS

In Figures 1 (no magnification) and 2 (40× magnification) are histologic slides of tissues stained with H&E. The normal thyroid gland consisted of round to oval thyroid follicles lined by a single layer of epithelial cells. Nucleoli were small, and chromatin was dense. Follicles contained eosinophilic colloid material and were separated by a small amount of benign adipose tissue.

C-Cell tumors were characterized by solid sheets of monotonous cells. There was much more cellular proliferation compared with the normal thyroid, and some areas were completely taken over by sheets of cells. The nuclear features were very characteristic of neuroendocrine cells. Chromatin was granular and dispersed, usually described as "salt and pepper" chromatin. Nucleoli were inconspicuous, and cytoplasm was barely visible. Large tumor masses had areas of necrosis and rather brisk mitotic activity.

Papillary thyroid carcinomas exhibited two main patterns. The complex papillary structures in some areas formed nodular masses (PTC) and in other areas had a follicular pattern (follicular variant papillary thyroid carcinoma [FV-PTC]). In both patterns, the follicles were lined by enlarged follicular cells. Nuclei were large, and chromatin was granular. There were optically clear nuclei and well-defined intra-nuclear pseudo-inclusions. Colloid material was either scant or absent. In other areas, the follicular lumen was obliterated by malignant cells. The cancer spread diffusely throughout the thyroids and was not contained to small nodules, as can be the case in human thyroid cancer.

In Figure 3 are B-mode images of mouse thyroids (normal and cancerous) along with QUS images enhanced by either the ESD or EAC. On B-mode images it would be difficult to differentiate between different thyroids on the basis of their visible appearance. However, through use of the QUS images, differentiation between the malignant and cancerous cases is possible. Nevertheless, thyroids containing benign C-cell adenomas could not be differentiated from normal thyroids on the QUS images.

Table 1 summarizes the average results for the different thyroid conditions examined. Scatter plots of ESD versus EAC and of ESD versus μ were also generated to illustrate the ability of QUS to differentiate thyroids

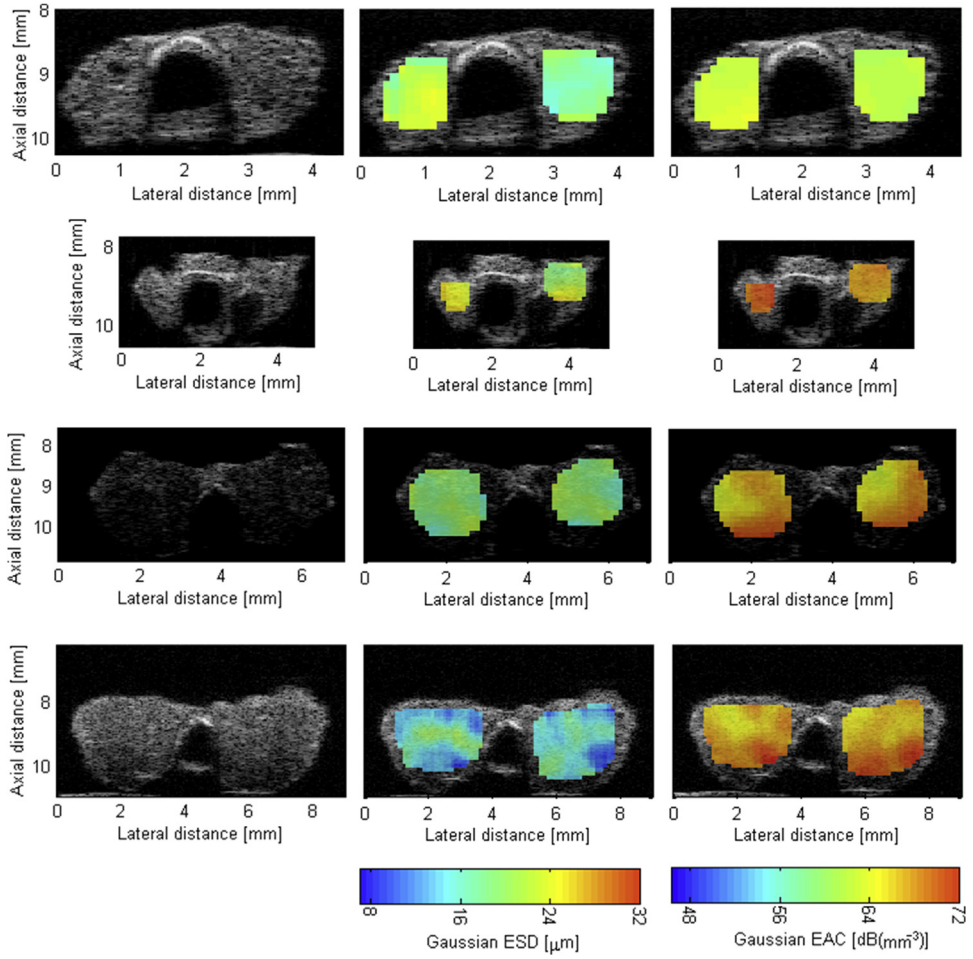

Fig. 3. B-Mode (left column) and quantitative ultrasound images of thyroids enhanced by (middle column) effective scatterer diameter (ESD) and (right column) effective acoustic concentration (EAC). Top row: normal thyroid (no tumor observed); second row: C-cell adenoma; third row: papillary thyroid carcinoma; bottom row: follicular variant papillary thyroid carcinoma.

(Figs. 4 and 5, respectively). The scatter plots indicate that different groups clustered together based on the values of the estimated parameters for each thyroid condition.

Given the relatively small population used in this study (*i.e.,* 25 animals in total), statistically significant differences between the different groups were estimated using the non-parametric Kruskal-Wallis test. Table 2 lists the *p*-values associated with the different sets of tumors and indicates statistically significant differences ($p < 0.05$) between the different kinds of thyroids scanned. Statistically significant differences were observed between the cancerous thyroids (PTC and FV-PTC) and the normal thyroids using the ESD, EAC, and μ parameters. The k parameter did not yield statistically significant differences between groups. No parameter was able to differentiate thyroids containing C-cell adenomas from normal thyroids. Only the ESD and EAC could differentiate cancerous thyroids from thyroids

Table 1. Estimated values of parameters for each thyroid condition examined

	ESD (μm)	EAC (dB mm^{-3})	k	μ
Normal	21.5 ± 1.80	52.9 ± 3.42	0.518 ± 0.07	1.56 ± 0.99
C-Cell adenoma	21.3 ± 1.50	54.7 ± 2.24	0.537 ± 0.12	1.96 ± 1.01
Papillary thyroid carcinoma	18.0 ± 0.92	59.4 ± 1.74	0.508 ± 0.05	2.55 ± 0.37
Follicular variant papillary thyroid carcinoma	15.9 ± 0.81	62.7 ± 1.61	0.558 ± 0.04	2.59 ± 0.43

ESD = effective scatterer diameter; EAC = effective acoustic concentration.

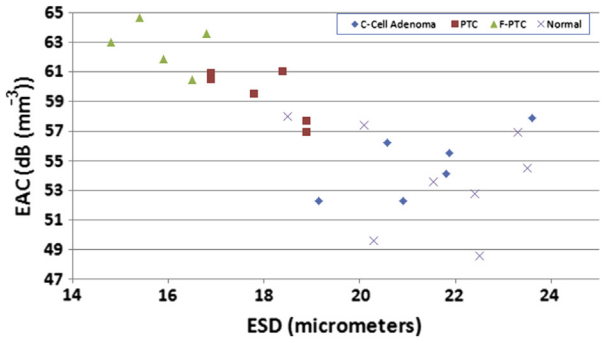

Fig. 4. Scatter plot of effective scatterer diameter (ESD) versus effective acoustic concentration (EAC) for the different kinds of thyroids examined. PTC = papillary thyroid carcinoma, FV-PTC = follicular variant papillary thyroid carcinoma.

containing C-cell adenomas. However, if the outlier for the C-cell adenoma in terms of the μ parameter is removed (see Fig. 5), then statistically significant differences are also observed between the cancerous thyroids and the thyroids containing C-cell adenomas. Finally, the ESD and EAC enabled PTC to be distinguished from FV-PTC. The μ parameter did not provide statistically significant differences between thyroids with PTC and those with FV-PTC.

DISCUSSION AND CONCLUSIONS

High-frequency QUS provided a new source of image contrast with the ability to differentiate cancerous thyroids in mice from both normal mouse thyroids and mouse thyroids with benign lesions (C-cell adenomas). Further, spectral-based QUS techniques enabled differentiation of the two types of cancerous thyroids. These results suggest that the additional information provided by QUS can improve the diagnostic potential of ultrasound for thyroid classification. Improving the ability of ultrasound to detect and classify thyroid cancer would greatly improve the management of thyroid cancer and could potentially alleviate the need for many biopsies.

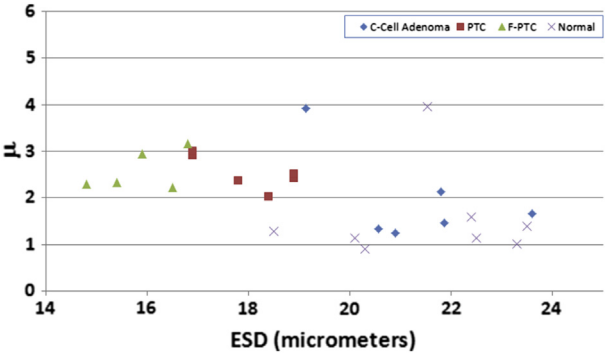

Fig. 5. Scatter plot of effective scatterer diameter (ESD) versus μ parameter for the different kinds of thyroids examined. PTC = papillary thyroid carcinoma, FV-PTC = follicular variant papillary thyroid carcinoma.

On comparison of the histologic slides of the different thyroid conditions examined with QUS parameters, some correlations were observed. The feature analysis plots in Figures 4 and 5 indicate that the ESD estimates are smallest for FV-PTC thyroids, medium for PTC thyroids, and largest for normal thyroids and those containing C-cell adenomas. From the histologic slides, the structure of normal thyroids is observed to be dominated by follicles. The follicles are lined by follicular cells, and the lumen contains colloid. Benign follicles varied from 40 to 100 μm in diameter. Benign cells measured approximately 10 μm in diameter. Malignant follicles varied from 60 to 200 μm in diameter, and malignant cells, from 15 to 24 μm in diameter. As cancer invaded the thyroid, the thyroid space became increasingly filled by malignant cells and less filled by follicles. If the scattering of ultrasound occurred from a combination of follicles and follicular cells, then as the thyroid tissue was taken over by the cancer, the scattering may have been more dominated by malignant cells, which are much smaller than follicles.

Furthermore, both EAC and μ were observed to increase from normal thyroid to cancerous thyroid. The increase in EAC means that the product of the number density and the impedance mismatch between the scatterer and background increased. The increase in μ corresponds to an increase in the number density of scatterers. In contrast to normal thyroids, cancerous thyroids are characterized by cellular hyperplasia. Assuming that the cells contribute significantly to the backscattered signal, this increase in the number of cells may result in an increase in the number of scatterers per unit volume. Therefore, an increase in the estimated number density (as reflected in both EAC and μ estimates) is consistent with an increased proliferation of cells observed in histologic analysis of the cancerous thyroids.

High-frequency QUS was required because the mouse thyroids were small (*i.e.,* only a few millimeters), and sufficient signal samples were needed to provide estimates of QUS parameters. The QUS parameters estimated from ultrasound signals over the frequency range 25–45 MHz produced contrast that allowed differentiation of malignant thyroids from normal thyroids or thyroids with benign growths. The high-frequency ultrasound used in these studies may have resulted in greater sensitivity to the microstructural changes occurring in cancerous thyroids compared with the normal thyroids. These microstructural changes were evident on the histologic slides of the different thyroids examined. Whether or not this contrast exists at more clinical ultrasound frequencies (1–20 MHz) has yet to be determined.

Table 2. p-Values from tests of statistically significant differences between groups for the ESD, EAC and μ parameters

	C-Cell adenoma				Papillary thyroid carcinoma				Follicular variant papillary thyroid carcinoma			
	ESD	EAC	μ	k	ESD	EAC	μ	k	ESD	EAC	μ	k
Normal	0.90	0.90	0.12	0.44	<0.05	<0.05	<0.05	0.27	<0.05	<0.05	<0.05	0.07
C-Cell adenoma					<0.05	<0.05	0.08	0.63	<0.05	<0.05	0.07	0.52
Papillary thyroid carcinoma									<0.05	<0.05	0.86	0.12

ESD = effective scatterer diameter; EAC = effective acoustic concentration.

However, because of the location of the thyroid gland in humans, it may be possible to use ultrasound signals at the higher end of the clinical ultrasound frequency range (~20 MHz). Furthermore, the contrast in QUS estimates detected in the mouse models of thyroid cancer may not translate into contrast in humans. Therefore, additional studies quantifying QUS contrast in human thyroid nodules are warranted.

Another difference between scanning of humans and scanning of the mouse thyroid samples used in this study is the use of excised tissue samples. The main objective of this study was to determine if there were significant differences in QUS parameters of normal and diseased thyroid tissues. Therefore, we decided to scan the thyroid glands *ex vivo* to eliminate effects caused by intervening tissues (*i.e.,* heterogeneous attenuation profiles, aberration, clutter, blood flow). In humans, thyroid nodules would be examined *in vivo,* and therefore, the aforementioned effects on the accuracy and precision of QUS estimates would need to be assessed.

Essentially, the radiofrequency backscattered signals from a whole thyroid lobe were used to produce an average QUS estimate for that particular thyroid sample. The justification for doing this was that histologically, the cancer in the thyroids appeared to be diffuse throughout most of the gland, as observed in Figure 1. The diffuse nature of the cancer in the diseased mouse thyroid may be partially attributable to the procedures used to monitor the progression of the disease. Mice were taken for QUS scanning and histology after the thyroids were enlarged as observed on sonograms obtained using the Vevo 2100 scanner. If the thyroids had been excised at earlier time points, it is possible that the cancer would have been less diffuse throughout the glands. On the other hand, it is still highly unlikely that in the cancerous cases, the whole thyroid lobe was affected by the malignancy. This could potentially increase the variance of estimates coming from malignant thyroids depending on how diffuse the disease was at the time of scanning. In humans with much larger thyroids and the potential to observe thyroid nodules, it may be possible to select signals only from suspicious thyroid lesion, thereby reducing the variance of QUS estimates and improving diagnostics.

This study has provided the first QUS results demonstrating significant contrast between cancerous thyroids and normal thyroids. However, it is a preliminary study, and many questions remain to be answered. Specifically, future work will focus on determining the QUS contrast in human thyroids at more clinical frequency ranges, modeling thyroid nodules in greater detail to correlate structural changes to QUS parameter estimates and providing QUS estimates from *in vivo* samples as opposed to excised samples. In addition, future studies should also include the estimation of attenuation from thyroid nodules to determine if attenuation can also be used to discriminate benign and malignant thyroid nodules.

Acknowledgments—The authors thank Rita Miller and Emily Hartman for their assistance in animal handling and scanning. This work was supported by a grant from NIH (R21 CA139095) and grants from Pontificia Universidad Católica del Perú (DGI2010-0105 and DGI2012-0149).

REFERENCES

Ahuja AT, Metreweli C. Ultrasound of thyroid nodules. Ultrasound Q 2000;16:111–121.

Ahuja A, Ying M. An overview of neck node sonography. Investig Radiol 2002;37:333–342.

American Cancer Society. Cancer facts and figures 2012. Atlanta, GA: American Cancer Society; 2012.

Brander AEE, Viikinkoski VP, Nickels JI, Kivisaari LM. Importance of thyroid abnormalities detected at US screening: A 5-y follow-up. Radiology 2000;215:801–806.

Catherine S, Maria L, Aristides A, Lambros V. Quantitative image analysis in sonograms of the thyroid gland. Nuclear Instrum Methods Phys Res Sect A 2006;569:606–609.

Chan BY, Desser TS, McDougall IR, Weigel RJ, Jeffrey RB Jr. Common and uncommon sonographic features of papillary thyroid carcinoma. J Ultrasound Med 2003;22:1083–1090.

Chen X, Phillips D, Schwarz KQ, Mottley JG, Parker KJ. The measurement of backscatter coefficient from a broadband pulse-echo systema: new formulation. IEEE Trans Ultrason Ferroelectr Freq Control 1997;44:515–525.

Chidiac RM, Aron DC. Epidemiology and clinical decision making. Endocrinol Metab Clin 1997;26:233–254.

Cooper DS, Doherty GM, Haugen BR, Kloos RT, Lee SL, Mandel SJ, Mazzaferri EL, McIver B, Pacini F, Schlumberger M, Sherman SI, Steward DL, Turtle RM. Revised American Thyroid Association management guidelines for patients with thyroid nodules and differentiated thyroid cancer. Thyroid 2009;19:1167–1214.

Cotran RS, Kumar V, Collins T. Pathologic Basis of Disease, 6 th Ed. Philadelphia, PA: W.B. Saunders Company, 1999.

Destrempes F, Cloutier G. A critical review and uniformized representation of statistical distributions modeling the ultrasound echo envelope. Ultrasound Med Biol 2010;36:1037–1051.

Feleppa EJ, Liu T, Kalisz A, Shao MC, Fleshner N, Reuter V, Fair WR. Ultrasonic spectral-parameter imaging of the prostate. Int J Imaging Syst Technol 1997;8:11–25.

Frates MC, Benson CB, Doubilet PM, Cibas ES, Marqusee E. Can color Doppler sonography aid in the prediction of malignancy of thyroid nodules. J Ultrasound Med 2003;22:127–131.

Fujii Y, Taniguchi N, Itoh K, Omoto K. Attenuation coefficient measurement in the thyroid. J Ultrasound Med 2003;22:1067–1073.

Ghoshal G, Lavarello RJ, Kemmerer JP, Miller RJ, Oelze ML. Ex vivo study of quantitative ultrasound parameters in fatty rabbit livers. Ultrasound Med Biol 2012;38:2238–2248.

Hruska DP. Improved techniques for statistical analysis of the envelope of backscattered ultrasound using the homodyned K distribution. Master's thesis, University of Illinois at Urbana-Champaign, 2009:29.

Hruska DP, Oelze ML. Improved parameter estimates based on the homodyned K distribution. IEEE Trans Ultrason Ferroelectr Freq Control 2009;56:2471–2481.

Iannuccilli JD, Cronana JJ, Monchik JM. Risk for malignancy of thyroid nodules as assessed by sonographic criteria. J Ultrasound Med 2004; 23:1455–1464.

Insana MF, Wagner RF, Brown DG, Hall TJ. Describing small-scale structure in random media using pulse-echo ultrasound. J Acoust Soc Am 1990;87:179–192.

Jacks T, Fazeli A, Schmitt EM, Bronson RT, Goodell MA, Weinberg RA. Effects of an Rb mutation in the mouse. Nature 1992;359:295–300.

Kim EK, Park CS, Chung WY, Oh KK, Kim DI, Lee JT, Yoo HS. New sonographic criteria for recommending fine-needle aspiration biopsy of nonpalpable solid nodules of the thyroid. Am J Roentgenol 2002;178:687–691.

Knauf JA, Ma X, Smith EP, Zhang L, Mitsutake N, Liao XH, Refetoff S, Nikiforov YE, Fagin JA. Targeted expression of $BRAF^{V600\ E}$ in thyroid cells of transgenic mice results in papillary thyroid cancers that undergo dedifferentiation. Cancer Res 2005;65:4238–4245.

Koike E, Noguchi S, Yamashita H, Murakami T, Ohshima A, Kawamoto H, Yamashita H. Ultrasonographic characteristics of thyroid nodules. Arch Surg 2002;136:334–337.

Lavarello R, Ghoshal G, Oelze ML. On the estimation of backscatter coefficients using single-element focused transducers. J Acoust Soc Am 2011;129:2903–2911.

Leinung MC, Gianoukakis A, Lee DW. Ultrasonography in management of nodular thyroid disease [letter to the editor]. Ann Intern Med 2001;135:383.

Lewis BD, Charboneau JW, Reading CC. Ultrasound-guided biopsy and ablation in the neck. Ultrasound Q 2002;18:3–12.

Liebeskind A, Sikora AG, Komisar A, Slavit D, Fried K. Rates of malignancy in incidentally discovered thyroid nodules evaluated with sonography and fine-needle aspiration. J Ultrasound Med 2005;24: 629–634.

Lizzi FL, Astor M, Liu T, Deng C, Coleman DJ, Silverman RH. Ultrasonic spectrum analysis for tissue assays and therapy evaluation. Int J Imaging Syst Technol 1997;8:3–10.

Mamou J, Coron A, Oelze ML, Saegusa-Beecroft E, Hata M, Lee P, Machi J, Yanagihara E, Laugier P, Feleppa EJ. Three-dimensional high-frequency backscatter and envelope quantification of cancerous human lymph nodes. Ultrasound Med Biol 2011;37:345–357.

Marqusee E, Benson CB, Frates MC, Doubilet PM, Larsen PR, Cibas ES, Mandel SJ. Usefulness of ultrasonography in the management of nodular thyroid disease. Ann Intern Med 2000;133: 696–700.

Mirilas P, Skandalakis JE. Benign anatomical mistakes: Incidentaloma. Am Surg 2002;68:1026–1028.

Moon WJ, Jung SL, Lee JH, Na DG, Baek JH, Lee YH, Kim J, Kim HS, Byun JS, Lee DH. Benign and malignant thyroid nodules: US differentiation—Multicenter retrospective study. Radiology 2008;247: 762–770.

Oelze ML, O'Brien WD Jr, Blue JP, Zachary JF. Differentiation and characterization of rat mammary fibroadenomas and 4 T1 mouse carcinomas using quantitative ultrasound imaging. IEEE Trans Med Imaging 2004;23:764–771.

Oelze ML, Zachary JF, O'Brien WD Jr. Characterization of tissue microstructure using ultrasonic backscatter: Theory and technique optimization using a Gaussian form factor. J Acoust Soc Am 2002;112:1202–1211.

Papini E, Guglielmi R, Bianchini A, Crescenzi A, Taccogna S, Nardi F, Panunzi C, Rinaldi R, Toscano V, Pacella CM. Risk of malignancy in nonpalpable thyroid nodules: Predictive value of ultrasound and color-Doppler features. J Clin Endocrinol Metab 2002;87: 1941–1946.

Rago T, Scutari M, Santini F, Loiacono V, Piaggi D, Di Coscio G, Basolo F, Berti P, Pinchera A, Vitti P. Real-time elastosonography: Useful tool for refining the presurgical diagnosis in thyroid nodules with indeterminate or nondiagnostic cytology. J Clin Endocrinol Metab 2010;95:5274–5280.

Rajendra Acharya U, Vinitha Sree S, Muthu Rama Krishnan M, Molinari F, Garberoglio R, Suri JS. Non-invasive automated 3-D thyroid lesion classification in ultrasound: A class of ThyroScan systems. Ultrasonics 2012;52:508–520.

Ross DS. Nonpalpable thyroid nodules: Managing an epidemic [editorial]. J. Clin. Endocrinol Metab 2002;87:1938–1940.

Sebag F, Vaillant-Lombard J, Berbis J, Griset V, Henry JF, Petit P, Oliver C. Shear wave elastography: A new ultrasound imaging mode for differential diagnosis of benign and malignant thyroid nodules. J Clin Endocrinol Metab 2010;95:5281–5288.

Silver RJ, Parangi S. Management of thyroid incidentalomas. Surg Clin North Am 2004;84:907–919.

Silverman RH, Folberg R, Rondeau MJ, Boldt HC, Lloyd HO, Chen X, Lizzi FL, Weingeist TA, Coleman DJ. Spectral parameter imaging for detection of prognostically significant histologic features in uveal melanoma. Ultrasound Med Biol 2003;29: 951–959.

Suzuki H, Willingham MC, Cheng S. Mice with a mutation in thyroid hormone receptor β gene spontaneously develop thyroid carcinomaa: Mouse model of thyroid carcinogenesis. Thyroid 2002;12: 963–969.

Tan GH, Gharib H. Thyroid incidentalomas: Management approaches to nonpalpable nodules discovered incidentally on thyroid imaging. Ann Intern Med 1997;126:226–231.

Vorlander C, Wolff J, Saalabian S, Lienenluke RH, Wahl RA. Real-time ultrasound elastography: A noninvasive diagnostic procedure for evaluating dominant thyroid nodules. Langenbecks Arch Surg 2010;395:865–871.

Wilson T, Chen Q, Zagzebski JA, Varghese T, VanMiddlesworth L. Initial clinical experience imaging scatterer size and strain in thyroid nodules. J Ultrasound Med 2006;25:1021–1029.